Korean J. Chem. Eng., 35(12), 2452-2463 (2018)
DOI: 10.1007/s11814-018-0131-8

pISSN: 0256-1115
eISSN: 1975-7220

Surface treatment of sol-gel bioglass using dielectric barrier discharge plasma to enhance growth of hydroxyapatite

Islam El-Sayed Soliman*,†, Asem El-Sayed Metawa,***, Mohamed Abdel Hameed Aboelnasr*, and Khairy Tohamy Eraba***

*Biophysics Branch, Faculty of Science, Al-Azhar University, Nasr City 11884, Cairo, Egypt
**Physics Department, Faculty of Science, Al-Azhar University, Nasr City 11884, Cairo, Egypt
***Physics Department, Faculty of Science, Al-Baha University, Al-Baha, Saudi Arabia
(*Received 26 April 2018 • accepted 26 July 2018*)

Abstract−Surface treatment of sol-gel bioglass is required to increase its biomedical applications. In this study, a dielectric barrier discharge (DBD) plasma treatment in atmospheric pressure was performed on the surface of [SiO_2-CaO-P_2O_5-B_2O_3] sol-gel derived glass. The obtained bioglass was treated by plasma using discharge current 12 mA with an exposure period for 30 min. The type of discharge can be characterized by measuring the discharge current and applied potential waveform and the power dissipation. Apatite formation on the surface of the DBD-treated and untreated samples after soaking in simulated body fluid (SBF) at 37 °C is characterized by Fourier transform infrared spectroscopy (FTIR), X-Ray diffraction (XRD), inductively coupled plasma (ICP-OES) and scanning electron microscopy coupled with energy dispersive spectroscopy (SEM/EDS). We observed a marked increase in the amount of apatite deposited on the surface of the treated plasma samples than those of the untreated ones, indicating that DBD plasma treatment is an efficient method and capable of modifying the surface of glass beside effectively transforming it into highly bioactive materials.

Keywords: Dielectric Barrier Discharge, Plasma Surface Treatment, Sol-gel Bioglass, Hydroxyapatite

INTRODUCTION

Bioactive glass is one of the biomaterials most used as implants for bone repair because of its high ability to facilitate the growth of hydroxycarbonate apatite (HCA) layer on its surface after implantation in a physiological environment [1]. The formation of HCA layer on the surface of biomaterials accelerates living tissue reactions to implanted material and facilitates additional attachment of cells, tissue growth factors and biomolecules [2]. Over the last few years, the main objective of most studies was to improve and accelerate body response to bioglass, which was carried out by several means such as adjusting its composition, changing preparation method, and using physical methods to modify the surface with no change in its original features. Therefore, more techniques have been developed [3-8] to modify the surface properties of bioglass, thereby helping to increase the apatite growth on its surface and thus enhancing the biocompatibility of these implants.

Bioactivity of glass can be regulated by changes in its chemical composition. However, the activation of bioactive glass in this study is controlled with surface treatment without any compositional changes. The range of composition is restricted since the change in chemical composition leads to variation in mechanical strength of the material and biocompatibility [3].

Erasmus et al. studied the effect of high temperature on crystallization and fabrication of porous bioactive glass sample, which consequently reduced its bioactivity [4]. Mačković et al. used flame spray method to produce 45S5 bioactive glass nanoparticles in which a mean particle size in the range of 20-60 nm was obtained [5]. 3D nanocomposite chitosan/bioactive glass scaffolds were fabricated by the sol-gel method by Lemos et al., where the results showed an increase in mechanical strength and bioactivity after the addition of bioactive glass, which was more pronounced when using the nanoscale bioactive glass. Khairy et al. prepared bioactive glass with B_2O_3 additive after which the samples showed less bioactivity at high boron content [7]. Yue et al. used a combination of chemical cross-linking and physical freeze-thawing methods to synthesize borate bioactive glass/PVA hydrogel composite with high strength [8]. Shaikh and Kedia treated 45S5 bioglass surface using femtosecond laser giving samples with high bioactivity [9]. So, there exists a requirement for a method to adjust the surface of glass samples to enhance its bioactivity. Here, we state our results of the current study we did on a number of bioactive glass samples that were prepared by sol-gel method and treated using a novel DBD plasma.

Despite the fact that biomedical sciences use lower-pressure plasma techniques more frequently instead of atmospheric-pressure, the latter is the most common, particularly in the field of plasma medicine. This field depends on the utilization of atmospheric plasma directly in living tissues, wound dressing, cancer therapy and other curative purposes [10]. Among the atmospheric pressure plasma sources, DBD is largely generally used in this field. DBD has several applications such as industrial ozone generation, surface modifications and sterilization of bacterial cells [11]. DBD can be per-

†To whom correspondence should be addressed.
E-mail: islam_biophysics@yahoo.com

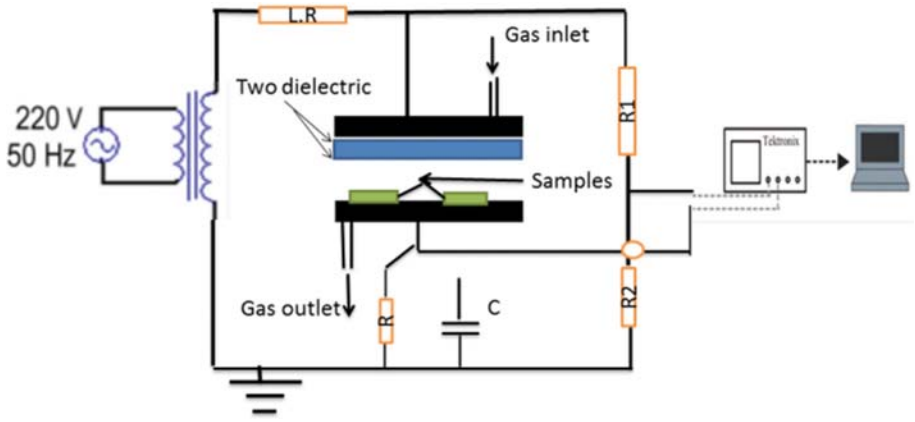

Fig. 1. Schematic diagram of the DBD experiment.

formed between two electrodes (the anode and cathode), one of them wrapped by a dielectric layer. The electrical attributes of DBD are subjected to several parameters such as the series capacitance contributed by the dielectric and varying air gap sandwiched by the electrodes, the frequency of the discharge voltages and dielectric material. At atmospheric pressure, the gas is ionized resulting in the formation of positive ions and free electrons [12].

Physical and chemical properties of material surface appreciably affect adhesion, wettability, anticorrosion, friction and light reflection [13]. Low-temperature and low-pressure oxygen plasma treatments are important for various reasons: they allow adjustment of the surface layers up to a profundity of a few nanometers from the surface without affecting the bulk properties of the substrate [14,15], they can attain the suitable surface polarities, damage to the sample can be avoided by treatment at low temperature [16], they are environmentally friendly [17], and they present new research fields, especially in biomaterial sciences.

More studies have been devoted to the application of surface treatment of plasma to tissue engineered scaffolds, especially in polymer and bioactive glass polymer composite. Simon et al. treated bioglasses and polymer composites with an air atmospheric pressure plasma process, and the formation and growth of HCA layer on the sample's surface took place [18]. Luo et al. treated 3-dimensional braided carbon fiber/polyetheretherketone (C3D/PEEK) composites by DBD plasma and found that the roughness increased, water contact angle decreased, new oxygen-containing functional groups were created on C3D/PEEK composite and a dense apatite layer formed which improved its bioactivity compared with the untreated samples [19]. In another study, biodegradable PLGA (70/30) films and scaffolds were treated with oxygen plasma and their results indicated that the apatite formability of this polymer was enhanced and apatite distribution became better in plasma-treated scaffolds than in untreated scaffolds [20]. In addition, Lebourg et al. proved that plasma was highly effective in the acceleration of apatite deposition on polycaprolactone sheets after plasma treatment when soaked in simulated body fluid [21]. Although there have been several studies on the bioactive glass, the effects of plasma treatment to the surface of bioactive glass without adding polymers are not frequently given. Therefore, our aim was to determine the effects of DBD plasma treatment on the growth of hydroxyapatite layer on the surface of SiO_2-CaO-P_2O_5-B_2O_3 sol-gel derived glass. The bioactivity test of plasma-untreated and treated samples was carried out in-vitro by soaking in simulated body fluid (SBF) at 37 °C for 15 days.

MATERIALS AND METHODS

1. Generation and Characterization of DBD Plasma

A schematic diagram of dielectric barrier discharge (DBD) for treatment of bioglass samples is shown in Fig. 1. The discharge was produced between two parallel plate electrodes, one covered by Pyrex glass and porous material plate with thickness 1.2 mm and radius 15 cm as a dielectric. The gap space between parallel plates was 2 mm. Oxygen plasma was sustained using the AC power supply (1-18 kV) operated at 50 Hz connected with the system. The electrical diagnostics of DBD was obtained by measuring the waveform of the discharge current and the Lissajous figures with applied potential across R=100 Ω, C=5 μF and potential divider (R_1=100 MΩ, R_2=100 kΩ). The signals from plasma were displayed on the digital storage oscilloscope. The power dissipation was calculated by measuring the charge on a 5 μF capacitor connected in series with the discharge chamber [22]. The bioglass with composition SiO_2-CaO-P_2O_5-B_2O_3 could be treated at 12 mA discharge current and the duration time of exposure for 30 min.

2. Bioglass Preparation and Characterization

2-1. Materials

Triethyl phosphate, [TEP, $OP(OC_2H_5)_3$] as P_2O_5 source, Calcium nitrate tetrahydrate [$Ca(NO)_3{\cdot}4H_2O$] as CaO source, Tetraethyl orthosilicate [TEOS, $Si(OC_2H_5)_4$] as SiO_2 source and Boric acid [H_3BO_3] as B_2O_3 were purchased from (Fluka). Nitric acid, 65%, and ammonia solution, 35%, were purchased from Merck, USA. All chemicals were obtained at ≥98% analytical grade. Ethanol C_2H_5OH was used as the solvent to prepare the sols and nitric acid as a catalyst. Both nitric acid and ammonia solutions were diluted to 2 M using distilled water.

2-2. Sample Preparation

The ternary gel glass system containing 70 wt% SiO_2 - 6 wt% P_2O_5 - 24 w% CaO was prepared by quick alkali-mediated sol-gel method and used as the control material [7]. B_2O_3 was added to bioglass compositions at the expense of SiO_2. Table 1 lists the nomi-

Table 1. The bioglass composition (weight ratio, %) and system abbreviation

X wt% B_2O_3	SiO_2	P_2O_5	CaO	Before soaking in SBF (G_{xb})	After soaking in SBF (G_{xa})	After soaking in SBF with plasma treatment (GT_{xa})
0	70	6	24	G_{0b}	G_{0a}	GT_{0a}
15	55	6	24	G_{15b}	G_{15a}	GT_{15a}
25	45	6	24	G_{25b}	G_{25a}	GT_{25a}

The compositions were abbreviated as G_{xb} and GT_{xa}, where (G) represents the glass, (x) indicate the ~%wt of the B_2O_3, (T) represents with treatment plasma, (b) represents before soaking in SBF and (a) represents after soaking in SBF

nal compositions and abbreviation of the prepared bioglass. Bioglass compositions were expressed after addition by the formula: [(70-X) SiO_2-6P_2O_5-24CaO-(X) B_2O_3, X=0, 15 and 25 wt%]. Initially, TEOS and 2 M nitric acid (as a hydrolysis catalyst) were progressively mixed in the presence of ethanol and distilled water. Then, the mixture was continuously stirred at room temperature for about 45 min to complete the hydrolysis and condensation reactions. The water to alkoxide molar ratio was fixed at 1/12 and water to nitric acid volume ratio was fixed at 1/6. The following reagents were added in sequence, permitting 45 min for each reagent to react completely: Ca $(NO)_3 \cdot 4H_2O$ and (TEP).

Boric acid was dissolved in distilled water separately; the molar ratio of water to H_3BO_3 was fixed at 15 : 1 at 40 °C for 30 min [23] under continuous stirring for the acid hydrolysis of H_3BO_3. Then we added this mixture to the first one. After the final addition, the mixtures were stirred for about 1 hr at room temperature to complete hydrolysis (clear sol). The final mixture was aged at room temperature for four days. Excess ammonia (2 M) solution (a gelation catalyst) was dropped into the acid sol in an ultrasonic water bath until gelation resulted. The obtained gel was stirred with glass rod (as a mechanical stirrer) to avoid forming a bulk gel. Finally, the resulting gel was kept at 120 °C for two days in a drying oven to remove the residual water and ethanol. The dry gel powders were calcined at 600 °C in air for 2 h to obtain stabilized glass according to the results of the thermal analysis showed by Tohamy et al. [7]. The heating rate of calcinations was fixed at 10 °C/min up to 600.

2-3. Sample Characterization

X-ray powder diffraction data were obtained using (XRD-model-Bruker AXS D8 ADVANCE), [Cukα=1.54056 Å] radiation. The prepared samples were milled in an agate mortar before testing. The operating conditions of X-ray tube were 40 kV and 40 mA, secondary monochromator settings in the 2θ ranged up to 70° at a step width of 0.02° with a count time of 0.4 s per step. The pattern was compared with the International Centre for Diffraction Data (PCPDFWIN Version 2.2 database of spectra and thus could be qualitatively identified, and Miller indexing (hkl) of the observed peaks. FTIR collected spectra of bioglass before and after immersion in SBF for 15 days were obtained at room temperature in the range of 4,000-400 cm^{-1} with a resolution of 2 cm^{-1}; using a Perkin-Elmer Model 580 IR spectrometer. The untreated and treated-plasma powder samples were mixed with previously dried KBr ratio of approximately 1 : 100. The mixture was then pressed into a transparent disc under 5 ton/cm^2. The surface morphologies of the specimens were observed by scanning electron microscope (SEM) (model XL30, Philips) operated at accelerating voltage of 30 kV. SEM micrographs were obtained after coating the specimens with a thin layer of gold because of the poor electrical conductivity of the specimens, using Edwards 5150 sputter coating, England, amplification image up to ×1,400 and its determination was (10 μm). The surface chemical analysis was carried out by energy dispersive X-ray spectroscopy (EDS) analysis. The wettability test of bioglass surface before and after plasma treatment was evaluated by water contact angle measurement. The contact angle is represented as the angle at which a liquid/vapor interface meets a solid surface. Sessile drop technique is used to calculate water contact angle by distilled water used as testing liquid at room temperature and relative humidity (23 °C and 50%, respectively). A 5 μL is the volume of the droplets for each test and droplets were kept for 30 s to reach a steady state before the measurement. At least three readings were taken for each sample during measurement and standard deviations were calculated from the mean value.

2-4. *In-vitro* Bioactivity of Bioglass in Simulated Body Fluid (SBF)

To evaluate the bioactivity of the prepared bioglass, the standard SBF solution with a composition close to that inorganic part of human plasma was prepared according to Kokubo's method. Reagent-grade chemicals were dissolved together in appropriate amounts of distilled water [24]. Each powder and disc forms of the obtained bioglass with and without plasma treatment was placed in one sterilized polyethylene bottle filled with SBF by a solid to liquid ratio of 10 mg/mL [25]. The samples were kept in this solution at 37 °C with pH 7.4 in a shaking-water bath for 15 without refreshing the immersing solution. The specimens were then removed from the SBF solution, rinsed with deionized water to prevent further reactions, and dried in air.

A 20 mL of SBF solution was taken from each sample and stored at 4 °C for inductively coupled plasma optical emission spectrometer (ICP-OES; Perkin Elmer 2100 OPTIMA DV, USA) analysis of Ca and P to determine the ionic concentration in SBF solution. The concentration was measured as a function of immersion time (1, 5, 10 and 15 days) using ICP. Each of these sample solutions was measured three times. The surface changes were then investigated through XRD, SEM, EDS, and FTIR techniques to determine the apatite-forming ability of bioglass with and without plasma treatment before and after soaking in SBF.

RESULTS AND DISCUSSION

1. DBD Plasma Characterization

1-1. Voltage-current Waveforms of O_2 Gas Discharge

The rates of processes of production of charged particles is influ-

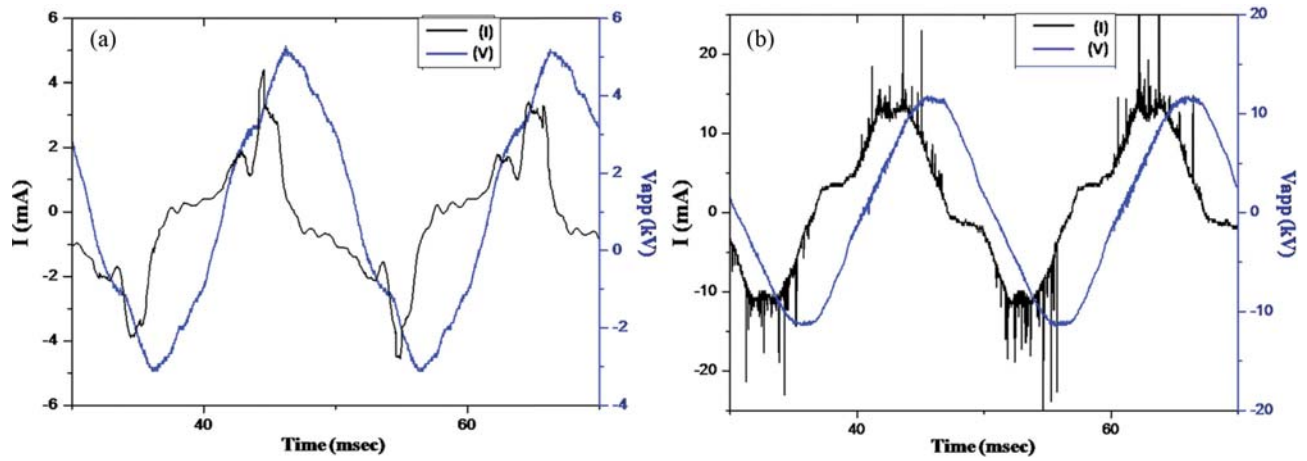

Fig. 2. Discharge current-voltage waveform in O_2 discharge at d=1 mm and f=50 Hz, (a) V_{ap}=5 kv (b) V_{ap}=12.2 kv.

enced directly by the waveform current of discharge. Fig. 2(a) shows waveforms of the applied potential to the discharge and the current of discharge at 2.0 mm reactor gap. The amplitude of the peak current is 5 mA and its rise time is about 3.5 msec, the current pulse magnitude in the quadrant of a cycle. The discharge current increase and the discharge voltage stable across the discharge gap, were attributed to increasing the ionization level to induce the formation of a cathode fall across the gap. Many electrons in the discharge gap were reversed sufficiently for producing the next breakdown under the low electric field, and thus for sustaining the atmospheric pressure glow discharge (APGD) [26].

By increasing the applied potential the discharge transition from the APGD to the filamentary discharge is shown typically in Fig. 2(b). The filamentary discharge has a large number of breakdown channels which were called (micro discharge) in the current waveform of plasma produced. From this figure, the current waveform consists of some filamentary with a duration time=3.5 msec. The different discharge regimes can be observed in O_2 plasma DBD such as the filamentary start to form inside the gap when the applied potential reaches the onset voltage value [27,28].

1-2. The Power Dissipation in the Discharge Measurements

The average discharge powers as functions of the applied potential for both glass and porous dielectrics are shown in Fig. 3. The power dissipation into plasma can be calculated from the Lissajous figures. The power increases from 5 W to 32 W by increasing in the applied potential increase from 5 kV to 12.2 kV. The increase of the applied potential leads to an increase in the number of microdischarges. Consequently, the average discharge power increases [29]. The discharge characteristics of the glass and porous dielectrics show that the discharge powers were mainly by the permittivity of the dielectric materials. The optimum condition for DBD with glass and porous dielectrics can be summarized in Table 2.

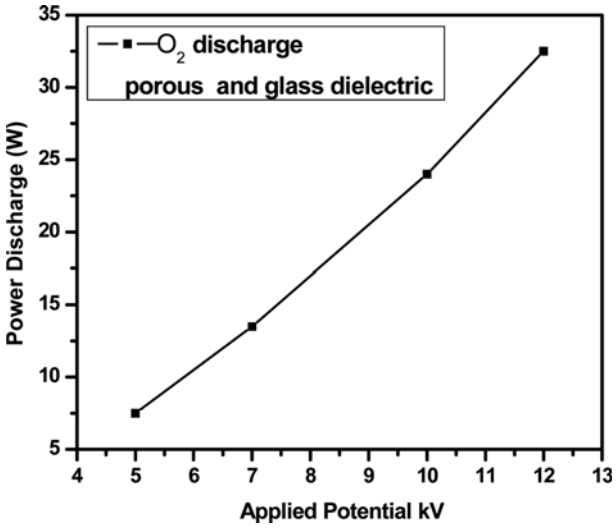

Fig. 3. The relation between applied voltage and power dissipation in O_2 discharge.

2. Characterization of Untreated and Plasma-treated Bioglasses

2-1. Surface Wettability

The water contact angle of bioglass was calculated to estimate the surface wettability of untreated and plasma-treated sample, as shown in Table 3. As can be noticed, all values of water contact angle before and after treatment were less than 90°, the water wets the surface and spreads over it (wettable), indicating a hydrophilic nature of the surface [30]. Furthermore, these results show that contact angle after plasma treatment was reduced significantly from 75 to 41, 70 to 32 and 64 to 38 leading to the surface of glass being more hydrophilic with good wettability. This increase in wettability is an important cause of induced growth of the apatite layer due to the formation of polar groups onto the surface of bioglass [31,32].

Table 2. Optimum condition of DBD plasma for treatment of bioglass surfaces

V_{app}	12.2 KV
Discharge current	12 mA
Power dissipation	32 W
Discharge type	Mixed from filamentary and glow discharge
Gas type	Oxygen
Dielectric capacitor	7.5 μF

Table 3. Water contact angle θ (in degree) (mean and standard deviation) of droplets on bioglass surfaces and apatite layer percentage formed on bioglass surface obtained with roughness analysis before and after plasma treatment

Sample	Plasma-untreated		Plasma-treated	
	Water contact angle (θ)	Apatite Percentage (%)	Water contact angle (θ)	Apatite Percentage (%)
0	75±0.4	67.91	41±0.5	83.11
15	70±0.16	79.71	32±0.34	95.43
25	64±0.5	48.62	38±0.7	75.19

This occurs as a result of the destruction of some Si-O bonds and alkali ions removal at the surface by DBD plasma, which enhances the generation of chemically active dangling bonds and hydroxyl groups at the surface of the silicon layer, thereby enhancing physical and chemical interactions between sample and biological fluid [33].

2-2. XRD

The observed XRD spectra before in vitro studies for all bioglasses without plasma treatment are shown in Fig. 4, which exhibit a dominant vitreous structure. All bioglasses have a broad amorphous halo beside the presence of a small diffraction peak for G_{0b} and G_{15b} but disappeared for G_{25b}. These peaks can be assigned to amorphous calcium phosphate phase (ACP) with chemical formula $Ca_4O(PO_4)_2$. This effect may be correlated with the assumption that ACP is precipitated after rapid mixing of aqueous solutions containing ions of calcium and orthophosphate [34].

The XRD spectra of untreated and plasma-treated bioglass after soaking in SBF for 15 days are shown in Fig. 5. In all plasma-untreated samples after soaking in SBF (Fig. 5(a)), three small peaks appear at 2θ values of 22.8°, 31.8° and 32.96°, which can be ascribed to (111), (211) and (300) reflections of hydroxylcarbonate apatite phase (HCA), together with a peak at 25.75° ascribed to the (002) reflection of calcium-deficient HCA according to the standard JCPDS cards (HCA, 82-1943). There is also a low diffraction peak observed at 2θ value 29.3° which is assigned to (104) reflection of

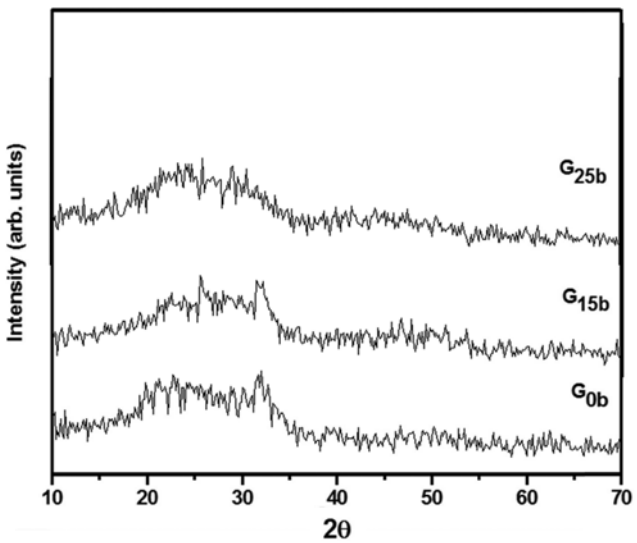

Fig. 4. XRD patterns of untreated-plasma bioglass before soaking in SBF.

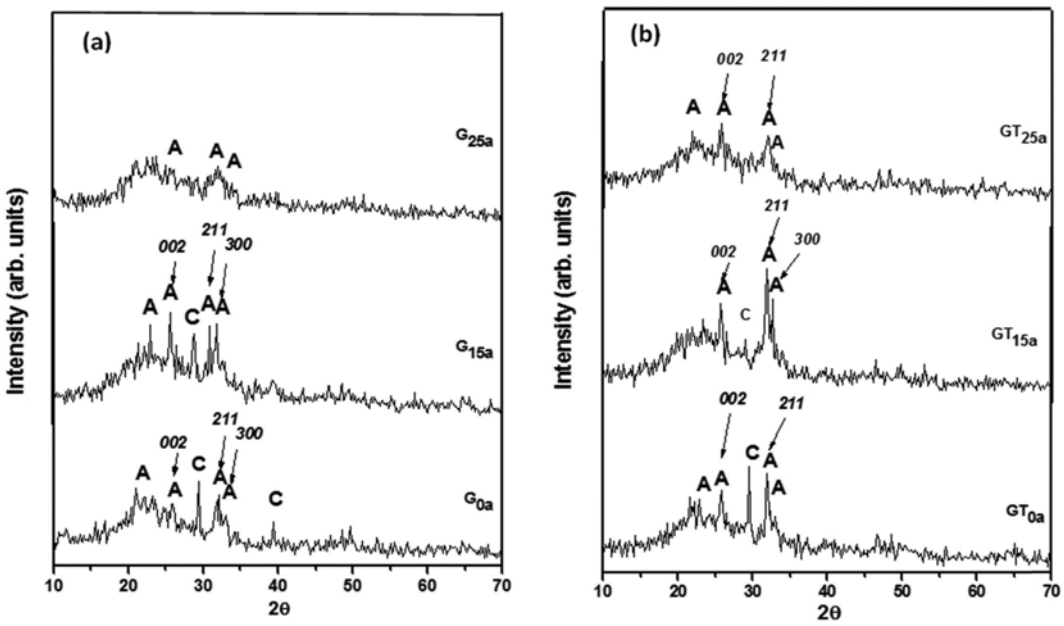

Fig. 5. XRD patterns of untreated (a) and plasma-treated (b) bioglass after soaking in SBF.

calcite ($CaCO_3$) according to the standard JCPDS card no (calcite, 81-2027) [35].

By comparing XRD patterns of the treated bioglass with those of the untreated one after soaking in SBF, as shown in Fig. 5(b), the intensity of the characteristic peaks associated with (002, 211 and 300) planes in treated samples is obviously stronger compared with the XRD patterns for the untreated samples, which is particularly evident in $GT_{15}a$ sample. This means that a higher growth of apatite layer occurs on the bioglass surface after being treated with DBD plasma. This variation in the amount of HCA layer formation on bioglass surface, before and after plasma treatment, takes place via the difference in dissolution and precipitation processes [36]. Therefore, nucleation site and crystal growth of the HCA phase are increased by increasing water contact angle leading to the surface of the sample being more wettable, thereby facilitating ionic interactions between bioglass surface and body fluid [37].

2-3. FTIR

Fig. 6 shows the FTIR spectra, in the range 'from 400-2,000 cm^{-1}', of untreated-plasma bioglass powder before soaking in the SBF solution. Sample (G_{0b}) boron-free, reveals characteristic absorption bands of silicate network located at 465 cm^{-1} (symmetric bending), 800 cm^{-1} (Si-O symmetric stretching of bridging oxygen atoms between tetrahedrons), 940 cm^{-1} (Si-O stretching of non-bridging oxygen atoms), and 1,070 cm^{-1} (Si-O-Si symmetric stretching). Furthermore, the absorption bands located at 562 cm^{-1}, 1,050 cm^{-1} and 1,212 cm^{-1} are related to a phosphate group and, respectively, ascribed to (P-O bending), (the symmetric bending vibration of PO_4^{3-}) and (the symmetric vibration of the P=O group) [38-40]. The band located at 680 cm^{-1} which is present in $G_{15}b$ and $G_{25}b$ is related to Si-O-B bending vibrations of B-O groups, which are not seen in boron-free G_0b sample [41].

Also, the band located at 800 cm^{-1} can be assigned to Si-O (BO), which gives a decrease in the intensity as B_2O_3 concentration is increased. Furthermore, a band appears at 940 cm^{-1}, which is attributed to $Si\text{-}O^-$ stretching in $[SiO_4]^{4-}$ tetrahedral units with three non-bridging oxygen (3NBO) atoms and silanol group in G_{0b} sample. On the other hand, this band appears obviously as a small shoulder due to linkages of B-O stretching vibration in BO_4 units with NBO atoms, and its intensity increases with increasing B_2O_3 contents in G_{5b} and G_{25b} samples [42-45].

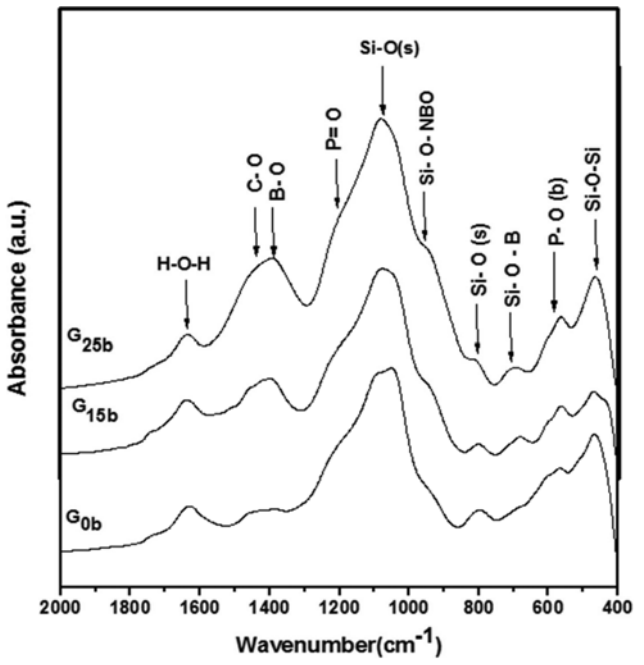

Fig. 6. FTIR spectra of untreated-plasma bioglass before soaking in SBF.

The 1,085 cm^{-1} band appears as a shift of 1,048 cm^{-1} band and covers contributions to form three bands. The first band is the symmetrical stretching vibration band of Si-O bond tetrahedral

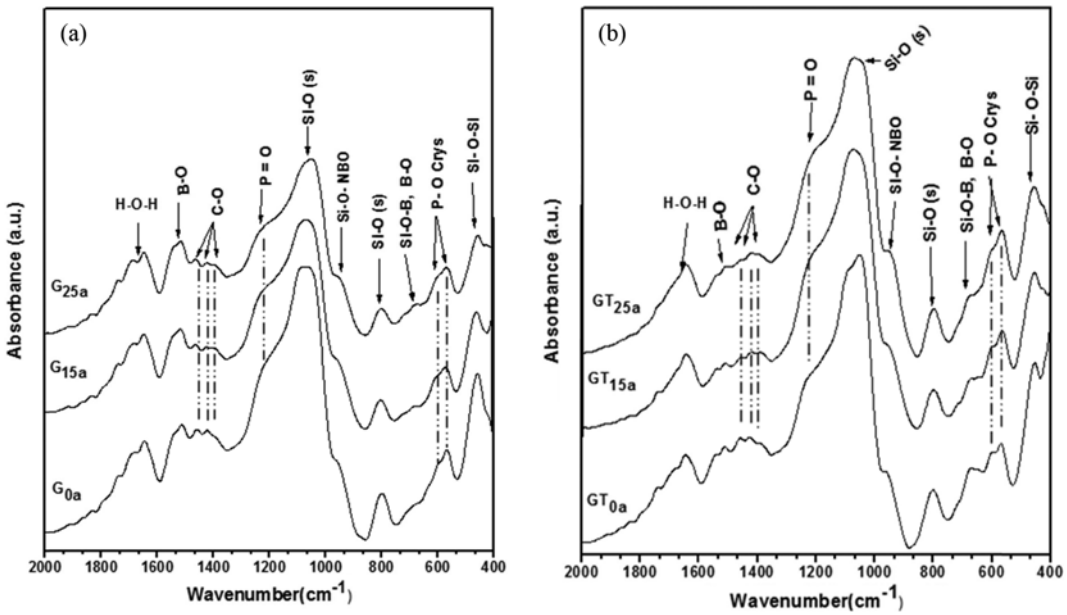

Fig. 7. FTIR spectra of plasma (a) untreated and treated (b) bioglass after soaking in SBF.

units. The second is B-O bond-stretching vibration band of BO_4 units from tri-, tetra- and penta-borate groups. Besides, the third is a symmetrical stretching vibration band of PO_3^{2-} terminal groups from pyrophosphate species [46]. The high frequency bands around 1,430 cm^{-1} increase with increasing of B_2O_3 in samples containing CaO. These bands indicate the presence of NBOs, which should have the forms of metaborate chains and rings, pyroborate and orthoborate groups [47], as shown in Fig. 6. A broad band located around 1,420 cm^{-1} is assigned to C-O stretching vibration mode in a carbonated group (CO_3^{2-}) [48]. In addition, a band appearing at 1,640 cm^{-1} is assigned to the bending mode of molecular water [7].

The FTIR can be used to verify the formation and growth of the apatite layer at the surface of the plasma-untreated and treated bioactive materials. In fact, taking into account that the apatite layer is characterized by the P-O bending vibration bands at 560 and 604 cm^{-1} and the P-O stretching vibration bands between 1,000 and 1,150 cm^{-1} [49]. The FTIR spectra of bioglasses after 15 days of soaking in SBF solution are shown in Fig. 7. In all plasma-untreated BG samples after soaking in SBF (Fig. 7(a)), amorphous P-O band located at 563 cm^{-1}, observed in all samples before soaking, split into two small bands at 564 cm^{-1} and 602 cm^{-1} after soaking in SBF. These two bands are assigned to crystalline P-O binding vibration mode of PO_4 group tetrahedra, thus indicative of the formation of a phosphate layer and prompt development of the surface apatite layer [50]. In addition, they appear with a higher degree of splitting and intensity after plasma treatment than those before plasma treatment. Moreover, P=O band located at 1,212 cm^{-1} appears as a small shoulder before plasma treatment. This band is increased in intensity and more well-defined after plasma treatment. Meanwhile, the carbonated band located at 1,420 cm^{-1} is resolved in three bands (1,390, 1,421 and 1,460 cm^{-1}) in all samples with and without treatment after soaking in SBF. These bands confirm the incorporation of carbonate ions from the solution in the apatite lattice, signifying the higher amount of carbonated apatite layer formed on the surface of bioglass samples. FTIR results are in agreement with other works [51-53].

The FTIR spectrum of the bone powder gives information about the crystallinity of the bone mineral-like apatite crystals. The concentrations of crystalline and amorphous apatite are calculated by Termine and Posner [54], known as percent crystallinity. The splitting factor (SF) (crystallinity index) of the prepared samples was calculated by drawing a baseline from 530-630 cm^{-1} and then measuring the heights of the 602 cm^{-1} (A) band and 563 cm^{-1} (B) band and dividing the sum value by the height of the hollow between them (C), corresponds to empirical formula (A+B)/C proposed by Weiner and Bar-Yosef [55].

Fig. 8 shows the difference in (SF) between glass samples with and without plasma treatment. After being soaked in SBF for 15 days, the SF values of glass sample after plasma treatment are higher than the sample before plasma treatment. These results suggest that the apatite-like layer formed on bioglass surface with plasma treatment possesses high crystallinity other than these samples without plasma treatment. This indicates that plasma treatment leads to enhancement of crystal growth of an amorphous calcium-phosphate phase, caused by destruction of some Si-O bonds and alkali ions removal. Therefore, the chemical stability of the system is disturbed, which causes a rearrangement of the bonds in the sample surfaces and increases the surface negativity of bioglass samples [56]. As a result, these groups act as sites of apatite nucleation, which facilitates the re-precipitation rate of Ca^{2+} and P^{5+} ions on the surface increased, and hence the formation rate of crystalline HCA phase is elevated.

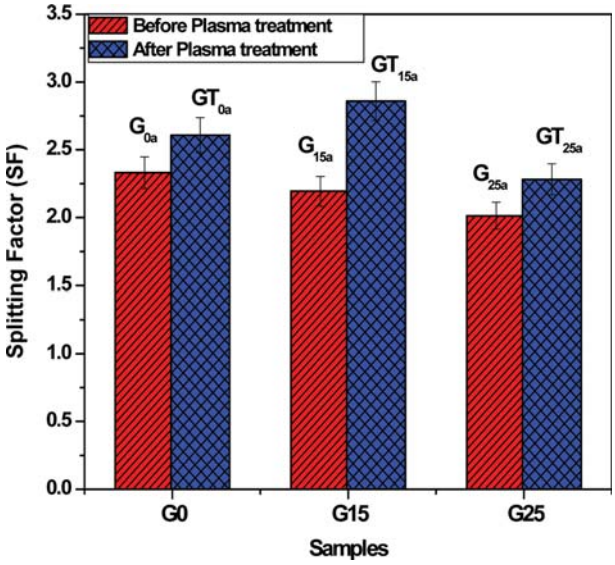

Fig. 8. SF values for all glass samples after soaking in SBF for 15 days with and without plasma treatment. The baseline was drawn from approximately 630-530 cm^{-1} for all heights.

2-4. *In-vitro* Dissolution in SBF Solution

The SBF solutions of the in-vitro analysis are examined by ICP-OES in order to describe Ca and P ions concentration. This analysis allows us to understand the ionic interactions between surface chemical groups of bioglass samples and the SBF solution. Fig. 9 shows the elemental concentrations of Ca and P of the SBF solutions containing untreated and plasma-treated samples, as a function of soaking time at 37 °C. It shows the profiles of degradation process of glass pellets in SBF. As Fig. 9 shows, before plasma treatment, Ca concentration in SBF solution increases from 103 to 320, 260 and 310 ppm for G_0a, $G_{15}a$ and $G_{25}a$ samples, respectively, in five days of soaking and then decreases gradually until the end of evaluating period. On the other hand, after plasma treatment, Ca concentration increases from 103 to 200, 175, and 230 ppm for GT_0a, $GT_{15}a$ and $GT_{25}a$ samples, respectively, during the first day of soaking and then decreases continuously until day 15. Moreover, P concentration decreases gradually from 33 ppm to 11, 9 and 7.5 ppm for G_0a, $G_{15}a$ and $G_{25}a$ treated samples, respectively, in 15 days of soaking, while P concentration of untreated samples decreases from 33 ppm to 5, 4 and 5.5 ppm for GT_0a, $GT_{15}a$ and $GT_{25}a$, respectively.

In general, the initial increase in Ca concentration is due to its release from the soaked sample. While, the subsequent decrease in Ca and P concentration is due to the precipitation of Ca and P ions, creating an apatite layer at the sample surface [57]. Dissolution curves show that the decrease in concentration of calcium and phosphorus ions with soaking time in treated samples is higher

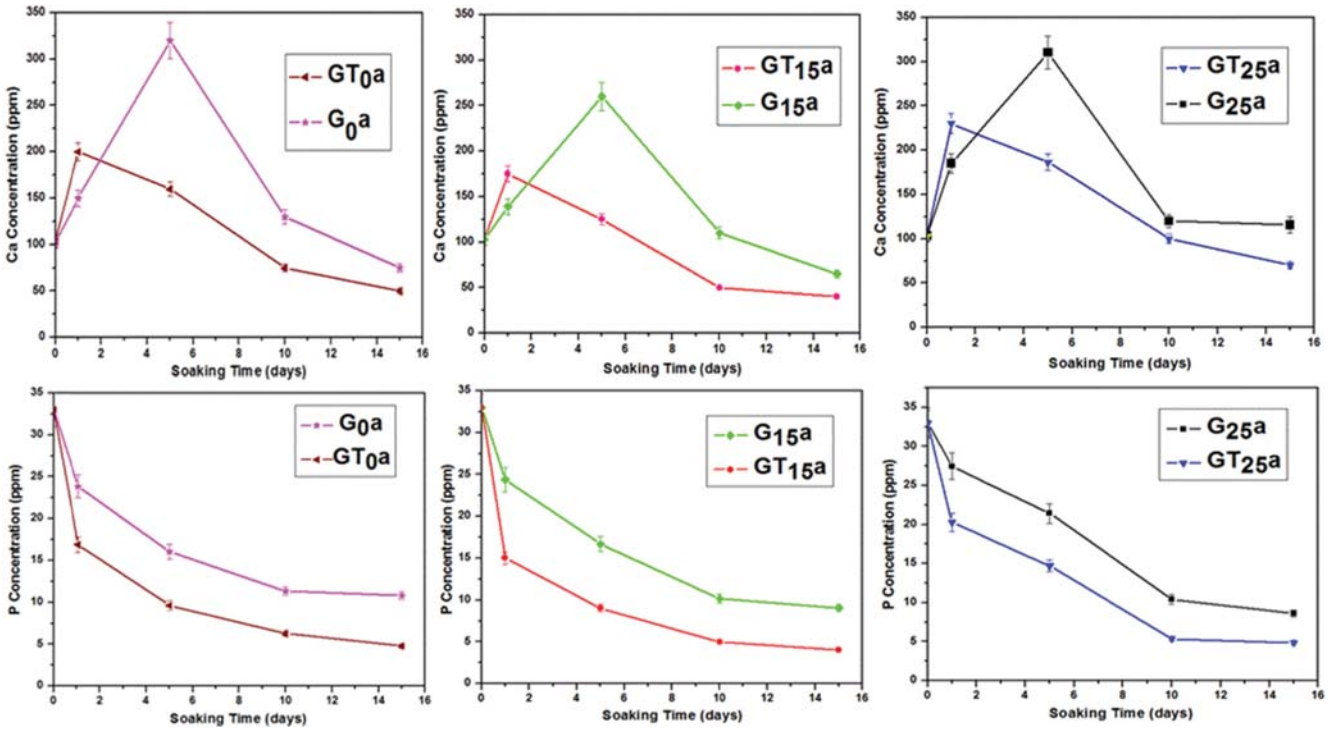

Fig. 9. Variation of calcium and phosphorus concentrations in the SBF solution with soaking time before and after plasma treatment.

than that of untreated samples. As is also evident, Ca concentration decreases after one day for all treated samples but in untreated samples it showed a decrease after five days. The number of Ca ions and timing of their migration from SBF solution to bioglass surface during precipitation process depends on whether their surface is plasma-treated or not. The early decrease in calcium ions concentration of treated samples is due to the large number of apatite nuclei formed rapidly on bioglass surface which, in turn, overcame the dissolution rate of Ca ions to the SBF solution [58]. This result clearly indicates that the rapid growth of apatite layer depends on the reaction between SBF and bioglass surface, which in turn has been affected by plasma treatment.

The apatite layer formation on bioglass surface involves three steps: ion exchange, dissolution, and precipitation. It is governed by the nucleation and crystal growth of particles during soaking period in the SBF solution [59]. These steps mainly depend on surface chemistry and morphology of the implanted bioglass [37]. Therefore, DBD plasma treatment can reduce the time taken to perform these three steps and thus accelerate nucleation and growth rate of an apatite layer on bioglass surface [60]. The results suggest that plasma treatment provides the hydrophilic properties to bioglass surface, thus allowing ions of SBF to interact with polar groups on the surface during formation of an initial site of apatite deposition [61]. These results are in agreement with the XRD, FTIR and surface wettability results.

2-5. SEM and EDS

The SEM micrograph of plasma-untreated bioglass G_{15b} before soaking SBF is shown in Fig. 10(a). The micrograph of the bioglass before soaking exhibits a relatively smooth surface without cracking and non-porous. The EDS analysis of bioglass surface results is

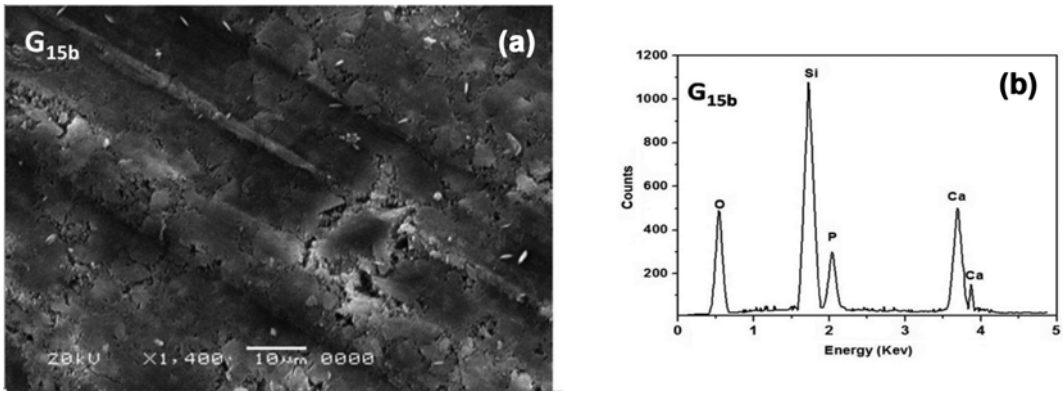

Fig. 10. (a) SEM image of prepared G_{15b} sample before soaking in SBF. (b) EDS patterns of glass G_{15b} sample before soaking in SBF.

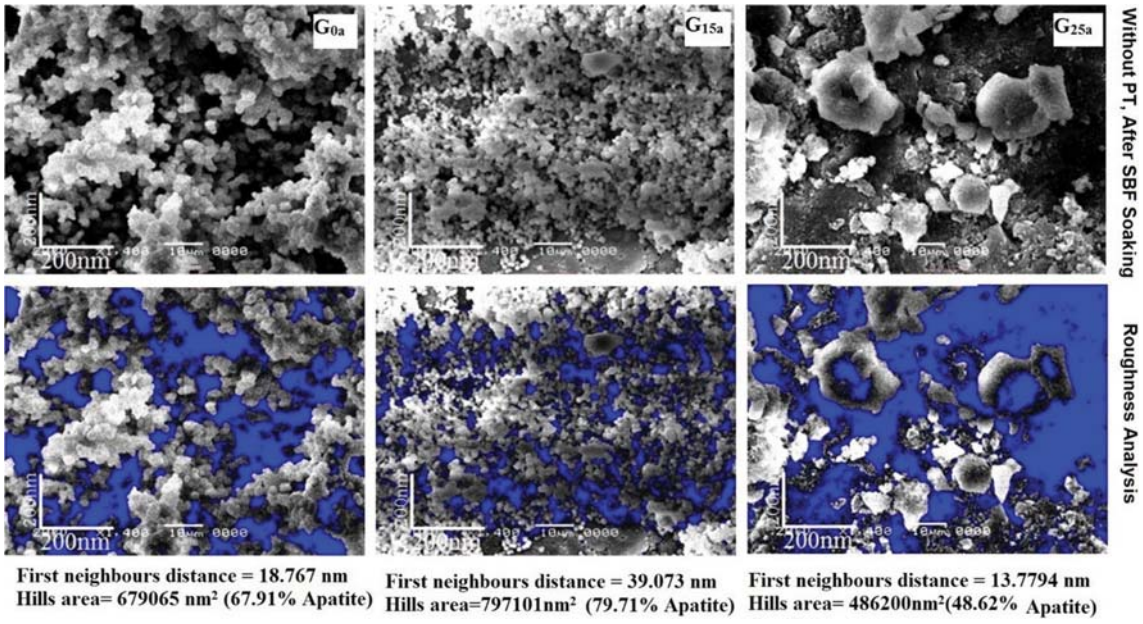

Fig. 11. (Top) SEM images of the bioglass samples G_{0a}, G_{15a} and G_{25a}. (Bottom) The same SEM images after treatment with the flooding algorithm in SXWM software. The blue areas represent the free-apatite sample surface.

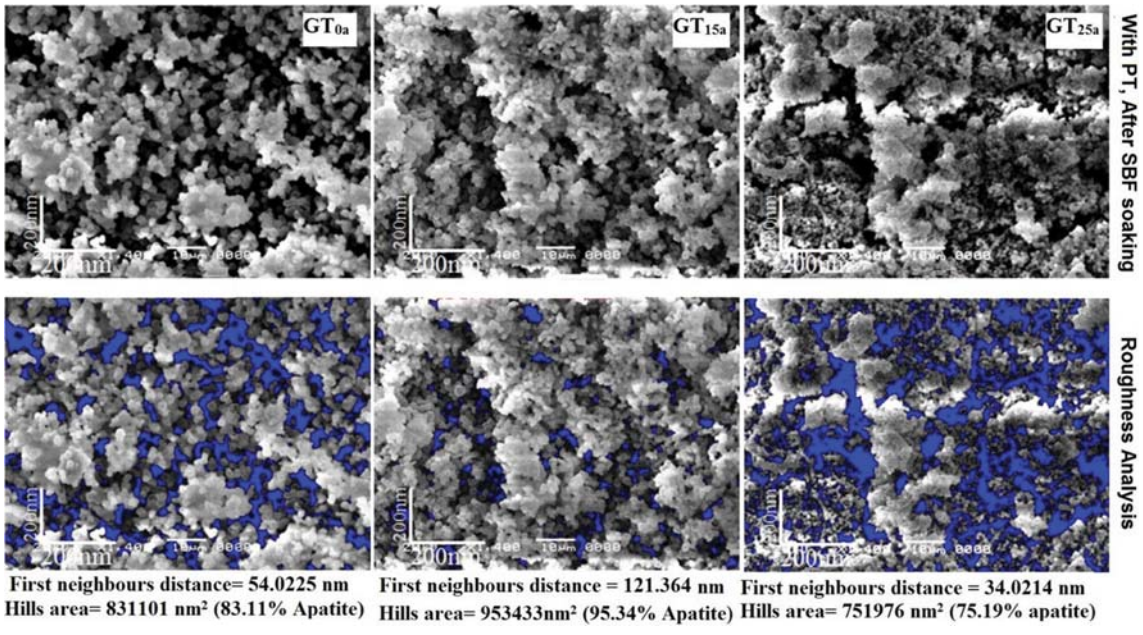

Fig. 12. (Top) SEM images of the bioglass samples GT_{0a}, GT_{15a} and GT_{25a}. (Bottom) The same SEM images after treatment with the flooding algorithm in SXWM software. The blue areas represent the free-apatite sample surface.

in good agreement with the nominal composition of the as-prepared bioglass given in Table 1.

SEM micrographs of plasma-untreated and treated bioglass samples after soaking in SBF solution for 15 days are shown in Fig. 11, 12. After soaking in SBF, modifications of plasma-untreated and treated bioglass surfaces are observed and the changes in ionic concentrations obtained by EDS analysis are recorded (Fig. 10(b), 13). The surface roughness of the sample was estimated using the SWXM program to show appreciable differences in the surface of treated and untreated-plasma samples after immersion in SBF solution [62].

After being soaked in SBF, the surfaces of all plasma-untreated samples were coated with cotton-like growth layer, composed of numerous spherical particles. These spherical particles are formed by small crystalline aggregates with particle size ranging from about 0.86-1.7 μm for each sample (Fig. 11). EDS spectra of this layer were observed to have a remarkable increase of calcium and phosphorus concentration, together with a significant decrease of the predominant silicon elements (Fig. 13). The decrease of silicon ions

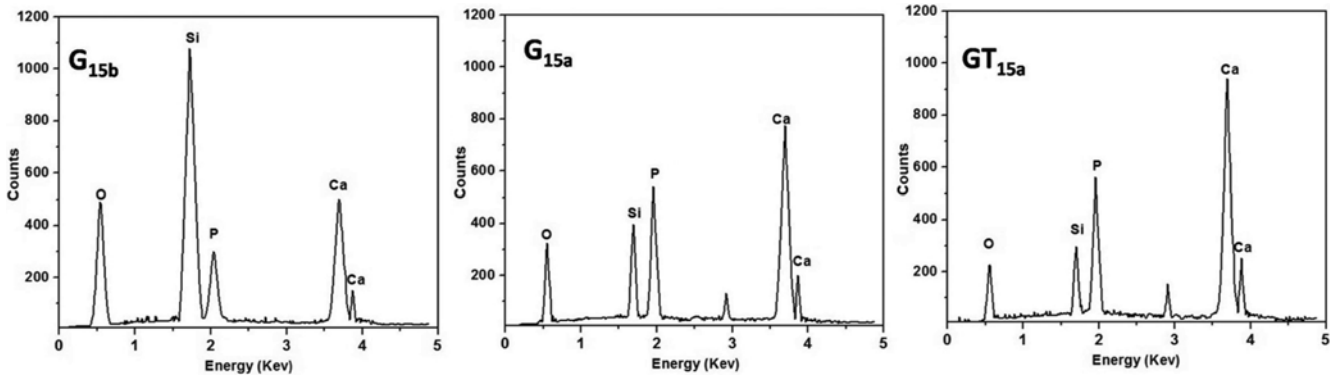

Fig. 13. EDS patterns of the layers formed on the bioglass samples G_{15b}, G_{15a} and GT_{25a}.

concentration with increasing Ca and P ions concentration suggests the formation of an apatite-like phase [38,63].

Moreover, compared with SEM micrographs taken for bioglass samples soaked in the SBF solution after plasma treatment for 30 min (Fig. 12) shows that there is a higher amount of an apatite layer precipitated on the surface of the samples. All samples fully covered with tiny spherical apatite particles with aggregates of approximately 10-15 μm in size were observed in different zones. The different morphologies give an indication of different precipitation of Ca and P ions present in these samples to form an HCA layer as previously mention by XRD and FTIR.

Another evidence to confirm the formation of an apatite layer on the bioglass surface sample before and after treatment is the EDS technique. Fig. 13 shows the data of EDS, where the spectra of these samples are compared. It is obvious that the both Ca and P peaks are enhanced for the DBD plasma-treated sample. Hence, the formed bone-like apatite layer is better distributed throughout the plasma-treated samples than the untreated samples [19,20].

A quantitative estimation of the apatite-covered areas is possible by employing the roughness analysis together with the flooding method algorithm in the SWXM software which allows the separation between the apatite phase and the bioglass surface. The blue areas in Fig. 11, 12 stand for the bioglass-free apatite areas. From Table 3, the values of the apatite percentage of plasma-treated samples GT_{0a}, GT_{15a} and GT_{25a} samples (~83.11%, 95.43% and 75.19%, respectively), are much higher than that of plasma-untreated samples GT_{0a}, GT_{15a} and GT_{25a} samples (~67.91%, 79.71% and 48.62%, respectively).

However, the addition of boron oxide beyond 25% has shown to lower the formation of an apatite layer (Table 3). The merit of plasma-treatment is clearly revealed in the enhancement of the apatite amount for the 25% boron sample from ~49% (before treatment) to ~80% (after treatment). Therefore, the plasma-treated samples, interestingly, combine the high percentage formation of apatite together with the high boron content in the sample.

The enhancement of apatite formation, which is evidenced by the obvious differences after plasma treatment, is due to the affected sample surface by DBD plasma and makes it a relatively rough surface. This increases the exposed surface area (i.e., increased number of interaction sites) and thus increases nucleation density at the surface, which facilitates the apatite-forming ability on the less bioactive glass surface [9]. A similar finding was reported by Qu et al. who declared that oxygen plasma treatment enhanced the number of negative charge and roughness of material's surface and increased their apatite nucleation ability when immersed in SBF [20]. Hence, it will be possible to improve the bioactivity of different glass compositions, which is difficult to increase its bioactivity by other methods, for example, by adding some elements in their composition leading to changes their physical and mechanical properties and thus affect their bioactivity. Therefore, we recommend using plasma treatment for such materials to control the surface treatment, while keeping the bulk properties unchanged.

CONCLUSION

The electrical characteristics of DBD were studied to determine the suitable conditions for effective operation of the DBD to the treatment of bioglass surface. Hence, controlled surface modification of bioglass was successfully established in atmospheric pressure at low temperature using DBD plasma. The observed changes in plasma-treated bioglass surface were quite different from those detected for untreated samples and were also confirmed by surface wettability, XRD, FTIR, dissolution test (ICP-OES), SEM and EDS. Water contact angle was reduced significantly after plasma treatment, leading to the surface of glass being more hydrophilic with good wettability. XRD analysis revealed that the typical diffraction patterns of the crystalline hydroxyapatite appeared with strong peaks on BDB plasma treated samples. Furthermore, FTIR results confirmed the appearance of relatively intense of doublets crystalline P-O bands, which are related to the formation of an apatite layer on BDB plasma treated bioglass. The dissolution test showed an early decrease in Ca ion concentration, which indicates the rapid formation of apatite nuclei formed on the treated samples that overcame the dissolution rate of Ca ions to the SBF. The SEM micrographs assured generation of microstructures on the bioglass samples after plasma treatment, which increases the surface roughness and hence the exposed surface area of the sample. This facilitates the apatite-forming ability on the less bioactive glass surface and uniform growth of HAP. However, obtained results show the high reactivity of the bioglass treated with DBD plasma after soaking for 15 days in SBF solution. DBD plasma surface treatment thus can be used as a potential technique enabling high growth

of good quality apatite phase deposited on this type of bioglass samples. Hence, new possibilities can be opened to enhance the bioactivity of the less bioactive glass by using DBD plasma to control surface treatment while maintaining bulk properties remain unchanged.

REFERENCES

1. L. L. Hench and J. R. Jones, *Front Bioeng Biotechnol.*, **3**, 194 (2015).
2. V. Stanić, Clinical Applications of Biomaterials; State-of-the-Art Progress, Trends, and Novel Approaches, G. Kaur, Eds., Springer International Publishing AG (2017).
3. I. Han, H. K. Baik, S.-W. Shin and I.-S. Lee, *Surf. Coat. Technol.*, **202**, 5746 (2008).
4. E. P. Erasmus, O. T. Johnson, I. Sigalas and J. Massera, *Scientific Reports*, **7**, 6046 (2017).
5. M. Mačković, A. Hoppe, R. Detsch, D. Mohn, W. J. Stark, E. Spiecker and A. R. Boccaccini, *J. Nanopart. Res.*, **14**, 966 (2012).
6. E. M. Lemos, P. S. Patrício and M. M. Pereira, *Química Nova*, **39**, 462 (2016).
7. K. M. Tohamy, I. E. Soliman, A. E. Motawea and M. A. Aboelnasr, *Nature Sci.*, **13**, 145 (2015).
8. T. Yue, L. Pang and D. Wang, *J. Non-Cryst. Solids*, **476**, 25 (2017).
9. S. Shaikh, S. Kedia, A. K. Singh, K. Sharma and S. Sinha, *J. Laser Applications*, **29**, 022004 (2017).
10. G. Fridman, G. Friedman, A. Gutsol, A. B. Shekhter, V. N. Vasilets and A. Fridman, *Plasm. Process. Polym.*, **5**, 503 (2008).
11. N. N. Morgan, *Int. J. Phys. Sci.*, **4**, 885 (2009).
12. R. Morent, N. De Geyter, T. Desmet, P. Dubruel and C. Leys, *Plasma Process. Polym.*, **8**, 171 (2011).
13. H. R. Yousefi, M. Ghoranneviss, A. R. Tehrani and S. Khamseh, *Surf. Interface Anal.*, **35**, 1015 (2003).
14. L. R. Shishoo, The 6th. Int. Conf. on Tex. Coat. & Lam., Dusseldorf, 35 (1996).
15. C. Pieter, R. Morent and N. De Geyter, Advances in Bioengineering, chapter 5, P. A. Serra Eds., IntechOpen pub., 117 (2015).
16. C. Labay, C. Canal, C. Rodríguez, G. Caballero and J. M. Canal, *Appl. Surf. Sci.*, **283**, 269 (2013).
17. C. Labay, J. M. Canal and C. Canal, *Plasma Process. Polym.*, **9**, 165 (2012).
18. A. Simon, O. Dinu, M. Papiu, V. Simon, H. Mocuta, J. Papp and S. D. Anghel, *Rom. Journ. Phys.*, **57**, 1392 (2012).
19. H. Luo, G. Xiong, K. Ren, S. Raman, Z. Liu, Q. Li, C. Ma, D. Li and Y. Wan, *Surf. Coat. Technol.*, **242**, 1 (2014).
20. X. Qu, W. Cui, F. Yang, M. Changchun, S. Hong, B. Jianzhong and W. Shenguo, *Biomaterials*, **28**, 9 (2007).
21. M. Lebourg, J. S. Antón and J. L. G. Ribelles, *Compos. Sci. Technol.*, **70**, 1796 (2010).
22. N. N. Morgan, A. Metawa and A. Garamoon, *Indian J. Phys.*, **85**, 1631 (2011).
23. R. L. Ciceo, D.-L. Trandafir, T. Radu, O. Ponta and V. Simon, *Ceram. Int.*, **40**, 9517 (2014).
24. T. Kokubo and H. Takadama, *Biomaterials*, **27**, 2907 (2006).
25. S. Hesaraki, M. Gholami, S. Vazehrad and S. Shahrabi, *Mater. Sci. Eng., C*, **30**, 383 (2010).
26. S. Gadkari and S. Gua, *Phys. Plasmas*, **24**, 053517 (2017).
27. R. Brandenburg, *Plasma Sources Sci. Technol.*, **27**, 1 (2018).
28. F. Weili, Z. Sheng, L. Dong, F. Liu, X. Zhong, Y. Cui, F. Hao and T. Du, *Sci. Rep.*, **7**, 8368 (2017).
29. A. Ozkan, T. Dufour, T. Silva, N. Britun, R. Snyders, A. Bogaerts and F. Reniers, *Plasma Sources Sci. Technol.*, **25**, 025013 (2016).
30. A. Elabid, G. Ying, S. Jianju, D. Ke and Z. Jing, *Plasma Sci. Technol.*, **18**, 346 (2016).
31. L. Hao and J. Lawrence, Laser Surface Treatment of Bio-Implant Materials, John Wiley & Sons, Ltd., 23 (2005).
32. F. Zhi, Q. Xiangqun, Q. Yuchang and K. Edmund, *IEEE Trans. Plas. Sci.*, **34**, 1216 (2006).
33. C. Seung-Woo, C. Woo-Beom, L. Yun-Hi and J. Byeong-Kwon, *J. Korea Phys. Soc.*, **38**, 207 (2001).
34. S. V. Dorozhkin, *Int. J. Mater. Chem.*, **2**, 19 (2012).
35. M. I. El-Gohary, K. M. Tohamy, M. M. El-Okr, A. F. Ali and I. E. Soliman, *Nature Sci.*, **11**, 26 (2013).
36. M. Mabrouk, M. M. Selim, H. Beherei and M. I. El-Gohary, *J. Gen. Eng. Biotechnol.*, **10**, 113 (2012).
37. K. Sharma, S. Kedia, A. K. Singh, C. B. Basak, A. K. Chauhan, S. Basu and S. Sinha, *J. Non-Cryst. Solids*, **440**, 43 (2016).
38. M. Mami, L.-G. Anita, H. Oudadesse, D.-S. Rachida, F. Mezahi and E. Dietrich, *Appl. Surf. Sci.*, **254**, 7386 (2008).
39. B. Lei, X. Chen, Y. Wang, N. Zhao, D. Chang and L. Fang, *J. Non-Cryst. Solids*, **355**, 2678 (2009).
40. H. Saeed, A. Masoud, N. Hamid and S. Davood, *J. Mater. Sci.: Mater. Med.*, **21**, 695 (2010).
41. T. Xiu, Q. Liu and J. Wang, *J. Solid State Chem.*, **181**, 863 (2008).
42. S. Agathopoulos, D. U. Tulyaganov, J. G. Ventura, S. Kannan, M. Karakassides and J. M. Ferreira, *Biomaterials*, **27**, 1832 (2006).
43. A. R. Boccaccini, Q. Chen, L. Lefebvre, L. Gremillard and J. Chevalier, *Faraday Discuss.*, **136**, 27 (2007).
44. R. S. Pryce and L. L. Hench, *J. Mater. Chem.*, **14**, 2303 (2004).
45. R. Ciceo-Lucaceo, D. Trandafir, T. Radu, O. Ponta and V. Simon, *Ceram. Int.*, **40**, 9517 (2014).
46. R. L. Ciceo and I. Ardelean, *J. Non-Cryst. Solids*, **353**, 2020 (2007).
47. K. S. Manupriya, K. Thind, V. Singh, V. Kumar, G. Sharma, D. Singh and D. Singh, *J. Phys. Chem. Solids*, **70**, 1137 (2009).
48. S. Hesaraki, M. Alizadeh, H. Nazarian and D. Sharifi, *J. Mater. Sci.: Mater. Med.*, **21**, 695 (2010).
49. C. Ohtsuki, H. Kushitani, T. Kokubo, S. Kotani and T. Yamamuro, *J. Biomed. Mater. Res.*, **25**, 1363 (1991).
50. X. Li, X. Wang, D. He and J. Shi, *J. Mater. Chem.*, **18**, 4103 (2008).
51. Z. Li, M. Al-Jawad, S. Siddiqui and J. D. Pasteris, *Sci. Rep.*, **5**, 16511 (2015).
52. C. Combes, S. Cazalbou and C. Rey, *Minerals*, **6**(2), 34 (2016).
53. S. Boulila, H. Oudadesse, H. Elfeki, R. Kallel, B. Lefeuvre, M. Mabrouk, S. Tounsi, D. Mhalla, A. Mostafa, K. Chaabouni, F. Makni-Ayedi, A. Barroug, T. Boudawara and A. Elfeki, *Korean J. Chem. Eng.*, **33**, 1659 (2016).
54. J. D. Termine and A. S. Posner, *Nature*, **211**, 268 (1966).
55. S. Weiner and O. Bar-Yosef, *J. Archaeological Sci.*, **17**, 187 (1990).
56. G. E. Stan, A. C. Popa and D. Bojin, *Digest J. of Nanomaterials and Biostructures*, **5**, 557 (2010).
57. A. A. El Hadad, E. Peón, F. R. García-Galván, V. Barranco, J. Parra, A. Jiménez-Morales and J. C. Galván, *Materials*, **10**, 94 (2017).
58. Y. Rezaei, F. Moztarzadeh, S. Shahabi and M. Tahriri, *Synth. React.*

Inorg. Metal-Orga. Nano-Meta. Chem., **44**, 692 (2014).
59. L. Jingyi, Y. Huijun and C. Chuanzhong, *RSC Adv.*, **8**, 2015 (2018).
60. R. A. Abdelrahim, N. A. Badr and K. Baroudi, *J. Inter. Soci. Preve. Comm. Dent.*, **6**, 15 (2016).
61. T. Yabutsuka, K. Fukushima, T. Hiruta, S. Takai and T. Yao, *Mater. Sci. Eng., C*, **81**, 349 (2017).
62. I. Horcas, R. Fernandez, J. M. Gomez-Rodrıguez, J. Colchero, J. Gomez-Herrero and A. M. Baro, *Rev. Sci. Instum.*, **78**, 013705 (2007).
63. V.-R. María and A. Ramila, *Chem. Mater.*, **12**, 961 (2000).